Supporting Information to the article

Recrystallization upon Solvent Vapor Annealing and Impact of Polymer Crystallinity on Hole Transport in Poly(3-hexylthiophene):Small Molecule Blends

Dorota Chlebosz[1,2], Krzysztof Janus[1,2], Kinga Danielewicz[2], Waldemar Goldeman[2], Agnieszka Czapik[3], Gunnar Glaßer[4], Markus Mezger[4], Adam Kiersnowski[1,2,*]

1. The Leibniz Institute of Polymer Research, Hohe Str. 6, 01069 Dresden, Germany
2. Wroclaw University of Science and Technology, Wyb. Wyspianskiego 27, 50-370 Wroclaw, Poland
3. Faculty of Chemistry, Adam Mickiewicz University, ul. Uniwersytetu Poznanskiego 8, 61-614 Poznań, Poland
4. Max Planck Institute for Polymer Research, Ackermannweg 10, 55128 Mainz, Germany

*correspondence: Adam Kiersnowski: kiersnowski@ipfdd.de; adam.kiersnowski@pwr.edu.pl

Keywords: poly(3-hexylthiophene), P3HT, aromatic dicarboximide, OFET, grazing-incidence, SEM

Table of contents:

1. Synthetic protocols and NMR spectroscopy of PIRnC6, NDInC4, NDInC6, NDInC8 and PDInC6

Materials. Imidazole >98% (product number I0001), pyromellitic dianhydride >98.0% (product number B0040) and naphthalene-1,4,5,8-tetracarboxylic dianhydride >97.0% (product number N0369) were purchased from TCI. Toluene, 96% ethanol, methanol and hydrochloric acid were obtained from a local supplier (Avantor). 3,4,9,10-perylenetetracarboxylic dianhydride 98% (product number 13008) from Acros organics, while n-butylamine 99.5% (product number 471305), n-hexylamine 99% (product number 219703), n-octylamine 99% (product number O5802) and chloroform >99.9% (CHROMASOLV®Plus, for HPLC, product number 34854) was supplied by Sigma-Aldrich. All reagents and solvents were used as received.

Preparation of PIRnC6: A mixture of pyromellitic anhydride (30 mmol, 6.5 g), n-hexylamine (90 mmol, 11.9 mL), imidazole (240 mmol, 16.4 g) and toluene (150 mL) was vigorously stirred and heated on oil bath for 12 hours at 150-160°C. After being cooled to room temperature (during cooling to room temperature the reaction mixture became thicker and more viscous, and finally forms a gel-like mass) the reaction mixture was evaporated to dryness to give a sticky residue. The residue was suspended in 96% ethanol (~300 mL) and poured into vigorously stirred cold 2N hydrochloric acid (~500 mL). Obtained suspension was filtered directly through thimble (Whatman™, 41 mm x 123 mm) and washed with methanol in a Soxhlet apparatus for 4 hours. Than the solvent was changed to chloroform and the extraction was continued until all soluble material was transferred to the flask. The chloroform solution (which forms a gel-like mass during cooling) was slowly and carefully (foam is formed) evaporated to dryness. Obtained gummy residue was purified by column chromatography (silica gel, CH_2Cl_2) and sublimation (180°C, $5 \cdot 10^{-2}$ mmHg), and finally PIRnC6 was obtained as white powder (3.2 g, 28%).

Preparation of NDInC4, NDInC6 and NDInC8: A mixture of naphthalene-1,4,5,8-tetracarboxylic dianhydride (15 mmol, 4.0 g), appropriate amine: n-butylamine (180 mmol, 17.8 mL), n-hexylamine (45 mmol, 6.0 mL) or n-octylamine (45 mmol, 7.4 mL), imidazole (120 mmol, 8.2 g) and toluene (75 mL) was vigorously stirred and heated on oil bath for 12 hours at 150-160°C. After being cooled to room temperature, the mixture was evaporated to dryness. Obtained residue was suspended in 96% ethanol (~150 mL) and poured into vigorously stirred cold 2N hydrochloric acid (~300 mL). The precipitate was filtered directly through thimble (Whatman™, 41 mm x 123 mm) and washed with methanol in a Soxhlet apparatus to remove any colored impurity and starting materials (extraction was continued until the washings became practically colorless). Than the solvent was changed to chloroform and the extraction was continued until all soluble material was transferred to the flask. The chloroform solution of the product was then evaporated to dryness, the residue was treated with methanol (50 ml),

filtered and dried on air yielded desired NDIs'. NDInC6 (5.3 g of the light pink powder, 82%) and NDInC8 (6.2 g of the light pink powder, 85%) were used without further purification, while NDInC4 (due to contamination of monoimide) was additionally purified by column chromatography (silica gel, CH_2Cl_2) and sublimation (200°C, $1.2 \cdot 10^{-2}$ mmHg). In result NDInC4 was obtained as beige powder (2.9 g, 51%).

Preparation of PDInC6: A mixture of perylene-3,4,9,10-tetracarboxylic dianhydride (15 mmol, 5.9 g), n-hexylamine (45 mmol, 6.0 mL), imidazole (120 mmol, 8.2 g) and toluene (75 mL) was vigorously stirred and heated on oil bath for 12 hours at 150-160°C. After being cooled to room temperature, the mixture was evaporated to dryness. Obtained residue was suspended in 96% ethanol (~150 mL) and poured into vigorously stirred cold 2N hydrochloric acid (~300 mL). The precipitate was filtered directly through thimble (Whatman™, 41 mm x 123 mm) and washed with methanol in a Soxhlet apparatus to remove any colored impurity and starting materials (extraction was continued until the washings became practically colorless). Than the solvent was changed to chloroform and the extraction was continued for about 96 hours (due to very low solubility of the PDInC6 it is a very time-consuming process. Furthermore, it has been observed that the extraction efficiency gradually decreased). After that, the suspension of crystallized product in chloroform was cooled to room temperature, filtered and dried on air yielded of the desired PDInC6 as tiny dark violet needles (7.5 g, 89%).

NMR Spectroscopy. The ^{1}H and ^{13}C NMR spectra were recorded on a 400 MHz Jeol ECZ 400S (PIRnC6) and 600 MHz Bruker Avance (NDInC4, NDInC6, NDInC8 and PDInC6) spectrometers in $CDCl_3$ or in the case of PDInC6 in $CDCl_3$+TFA (5:1, V/V) as solvent. Chemical shifts (δ) are given in parts per million (ppm) relative to solvent signals (7.26 ppm and 77.2 ppm in ^{1}H NMR and ^{13}C NMR spectra, respectively). Multiplicity is described as follows: s=singlet, t=triplet, q=quartet, quint=quintet, sext=sextet, m=multiplet.

N,*N*'-di(n-hexyl)benzene-1,2,4,5-tetracarboxylic diimide (**PIRnC6):** ^{1}H NMR (400MHz, $CDCl_3$) δ: 0.86 (t, 6H, *J*=7.6 Hz, CH_3), 1.23-1.38 (m, 12H, $CH_3(\underline{CH_2})_3$), 1.68 (quint, 4H, *J*=7.2 Hz, $\underline{CH_2}CH_2N$), 3.72 (m (AA'XX' spin system), 4H, CH_2N), 8.24 (s, 2H, ArH); ^{13}C NMR (100MHz, $CDCl_3$) **δ**: 14.05, 22.56, 26.56, 28.46, 31.36, 38.82, 118.17, 137.32, 166.39. ^{1}H and ^{13}C NMR spectra are in agreement with the literature data.[1]

N,*N*'-di(n-butyl)naphthalene-1,4,5,8-tetracarboxylic diimide (**NDInC4**): ^{1}H NMR (600MHz, $CDCl_3$) δ: 1.02 (t, 6H, *J*=7.2Hz, CH_3), 1.48 (sext, 4H, *J*=7.2Hz, $CH_3\underline{CH_2}$), 1.76 (m, 4H, $\underline{CH_2}CH_2N$), 4.22 (m (AA**'** XX**'** spin system), 4H, CH_2N), 8.75 (s, 4H, ArH); ^{13}C NMR (151MHz, $CDCl_3$) δ: 13.81, 20.24, 30.06,

40.75, 126.63, 126.68, 130.91, 162.79. ^{1}H and ^{13}C NMR spectra are in agreement with the literature data.[2, 3]

N,*N*'-di(n-hexyl)naphthalene-1,4,5,8-tetracarboxylic diimide (**NDInC6**): ^{1}H NMR (600MHz, $CDCl_3$) δ: 0.92 (t, 6H, *J*=7.2 Hz, CH_3), 1.33-1.41 (m, 8H, $CH_3(\underline{CH_2})_2$), 1.46 (quint, 4H, *J*=7.2 Hz, $\underline{CH_2}(CH_2)_2N$), 1.77 (m, 4H, $\underline{CH_2}CH_2N$), 4.22 (m (AA' XX' spin system), 4H, CH_2N), 8.78 (s, 4H, ArH); ^{13}C NMR (151MHz, $CDCl_3$) δ: 14.04, 22.55, 26.74, 28.02, 31.49, 40.98, 126.59, 126.62, 130.88, 162.76. ^{1}H and ^{13}C NMR spectra are in agreement with the literature data.[4, 5]

N,*N*'-di(n-octyl)naphthalene-1,4,5,8-tetracarboxylic diimide (**NDInC8**): ^{1}H NMR (600MHz, $CDCl_3$) δ: 0.90 (t, 6H, *J*=7.0 Hz, CH_3), 1.25-1.35 (m, 12H, $CH_3(\underline{CH_2})_3$), 1.39 (m, 4H, $\underline{CH_2}(CH_2)_3N$), 1.45 (m, 4H, $\underline{CH_2}(CH_2)_2N$), 1.76 (m, 4H, $\underline{CH_2}CH_2N$), 4.21 (m (AA'XX' spin system), 4H, CH_2N), 8.77 (s, 4H, ArH); ^{13}C NMR (151MHz, $CDCl_3$) δ: 14.09, 22.63, 27.02, 28.08, 29.04, 29.29, 31.80, 40.59 126.60, 126.64, 130.88, 162.77. ^{1}H and ^{13}C NMR spectra are in agreement with the literature data.[2, 6]

N,*N*'-di(n-hexyl)perylene-3,4,910-tetracarboxylic diimide **(PDInC6)**: ^{1}H NMR (600MHz, $CDCl_3$/TFA, 5:1, V/V) δ: 0.95 (t, 6H, *J*=7.2 Hz, CH_3), 1.36-1.44 (m, 8H, $CH_3(\underline{CH_2})_2$), 1.49 (quint, 4H, *J*=7.2Hz, $\underline{CH_2}(CH_2)_2N$), 1.79 (m, 4H, $\underline{CH_2}CH_2N$), 4.24 (m (AA'XX' spin system), 4H, CH_2N), 8.55 (d, 4H, *J*=7.8 Hz, ArH), 8.66 (d, 4H, *J*=7.8 Hz, ArH), 11.25 (s, CF_3COOH); ^{13}C NMR (151MHz, $CDCl_3$/TFA, 5:1, V/V) δ: 13.59, 22.38, 26.56, 27.77, 31.29, 41.74, 114.22 (q, $^{1}J_{CF}$ = 285.1 Hz, CF_3COOH), 122.18, 123.91, 125.82, 128.88, 132.59, 135.02, 161.52 (q, $^{2}J_{CF}$ = 42.9 Hz, CF_3**C**OOH), 164.81. ^{1}H and ^{13}C NMR spectra are in agreement with the literature data.[6]

2. Molecular structures, crystallographic data and energy levels of ADI used in the basic and extended studies

Table S1. Crystallographic and molecular data of ADIs used in the basic and extended studies

Molecule	**P3HT**	**PIRnC6**	**NDInC4**[2]	**NDInC6**[8,9]	**NDInC8**	**PDInC6**[7]
Molar mass / g×mol^{-1} (polydispersity index)	M_w :60×10^3 (22)	384.5	378.4	434.5	490.6	558.7
Alkyl to aromatic ratio, $I_{\alpha/\alpha}$	1.2	2.0	0.8	1.2	1.8	0.7
solubility parameters, δ /MPa$^{1/2}$	**δ_t=19.4** δ_d=19.4; δ_p= 1.7; δ_h=0.7;	**δ_t=18.1** δ_d=18.0; δ_p=1.5; δ_h=-1.9;	**δ_t=19.8** δ_d=19.6; δ_p=2.0; δ_h=-1.4;	**δ_t=19.6** δ_d=19.5; δ_p=1.4; δ_h=-1.9;	n/a	n/a
Crystal structure	**monoclinic**	**triclinic**	**triclinic**	**triclinic**	**triclinic**	**triclinic**
Crystal system	$P2_1/c$	$P\bar{1}$	$P\bar{1}$	$P\bar{1}$	$P\bar{1}$	$P\bar{1}$
a / Å	···16.3···	···5.69···	···5.32···	···4.90···	···4.77···	···4.72···
b / Å	···7.6····	···10.2···	···8.04···	···8.28···	···6.53···	···8.52···
c / Å	···7.7···	···18.9···	···11.2···	···14.5···	···22.7···	···17.3···
α / °	···90.0···	*···94.4··*	*···103.7··*	*···96.3···*	*···88.0···*	*···81.3···*
β/ °	···90.0···	*···96.8···*	*···94.4···*	*···98.1···*	*···89.0···*	*···85.8···*
γ/ °	···87.0···	*···90.2···*	*···95.2···*	*···93.6···*	*···75.8···*	*···83.9···*
CSD Refcode / CCDC#		1998574 1998577	819749	671518 804310	1998575 1998576	1896752
Band gap	LUMO -2.7 eV HOMO -4.9 eV	LUMO -3.6 eV HOMO -7.1 eV	LUMO -3.6 eV HOMO -7.3 eV	LUMO -3.6 eV HOMO -7.3 eV	LUMO -3.6 eV HOMO -7.2 eV	LUMO -3.8 eV HOMO -6.2 eV

3. Blend component ratios and solution concentrations

Table S2. Component ratios and concentrations in chloroform solutions of all the blends in the study

Components	P3HT:ADI ratio	ADI wt. fract. in the blend	conc. of P3HT in solution [mg/mL]	total sol. conc. [mg/mL]
P3HT	**1:0**	**0.00**	**1.00**	**1.00**
P3HT:PIRnC6	**2:1**	**0.33**	**1.00**	**1.51**
P3HT:PIRnC6	**1:2**	**0.66**	**1.00**	**3.00**
P3HT:PIRnC6	**1:16**	**0.94**	**1.00**	**17.00**
PIRnC6	**0:1**	**1.00**	**0.00**	**5.04**
P3HT:NDInC4	9:1	0.10	1.00	1.12
P3HT:NDInC4	2:1	0.38	1.00	1.60
P3HT:NDInC4	1:9	0.90	1.00	10.30
NDInC4	0:1	1.00	0.00	4.99
P3HT:NDInC6	**2:1**	**0.33**	**1.00**	**1.52**
P3HT:NDInC6	**1:3**	**0.75**	**1.00**	**4.02**
P3HT:NDInC6	**1:16**	**0.94**	**1.00**	**17.05**
NDInC6	**0:1**	**1.00**	**0.00**	**5.05**
P3HT:NDInC8	2:1	0.33	1.00	1.51
P3HT:NDInC8	1:8	0.89	1.00	9.05
P3HT:NDInC8	1:40	0.98	1.00	41.01
NDInC8	0:1	1.00	0.00	5.02
P3HT:PDInC6	**37:1**	**0.03**	**1.00**	**1.03**
P3HT:PDInC6	**25:1**	**0.04**	**1.00**	**1.04**
P3HT:PDInC6	**5:1**	**0.17**	**1.00**	**1.21**
PDInC6	**0:1**	**1.00**	**0.00**	**0.17**

4. Exemplary current-voltage characteristics, the method to extract working OFET parameters

OFET were characterized by measuring output (U_{DS}, U_{GS} ranging from +10 to -80 V or from -10 to +80 V) and transfer (U_{DS} = ± 80 V, U_{GS} ranging from +10 to -80 V or from -10 to +80 V) current-voltage characteristics – the sign of voltages was negative for hole current measurements and positive for electrons.

Charge carrier mobilities were calculated from the slopes of transfer characteristics $I_{DS}^{1/2}$ vs U_{GS}. For nonlinear characteristics linear fits were calculated for the highest gate voltages – this makes the calculated mobilities less affected by the unintentional doping effect that may influence current measured at low U_{GS}. The common equation was used:

$$\mu_h = \left(\frac{dU_{DS}^{1/2}}{dU_{GS}}\right) \cdot \frac{2L}{W \cdot C}$$

where L and W stand for channel length and width, while C is surface capacitance of the dielectric layer. These parameters were equal to 40 μm, 1000 μm and 11.5 nF/cm^2, respectively.

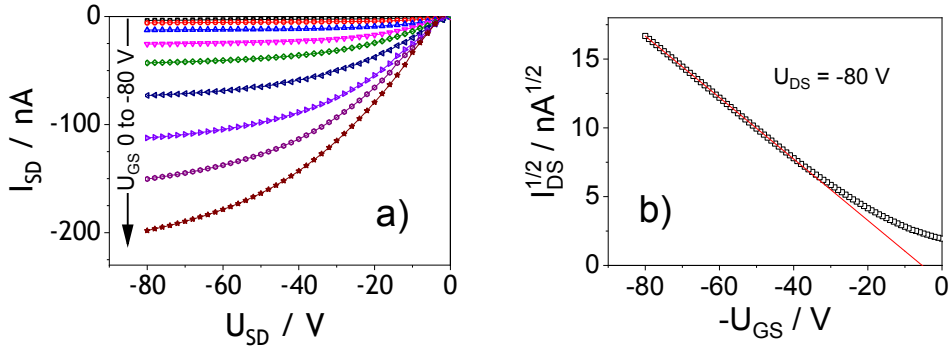

Figure S1. Exemplary output (a) and transfer (b) characteristics of OFET (here P3HT:PIRnC6, 1:16 blend). The straight line fitting the transfer characteristics which slope was used for mobility determination is indicated in figure B.

5. Extended studies on OFET hole mobility in P3HT:ADI blends, and electron mobilities determined for the materials in the study

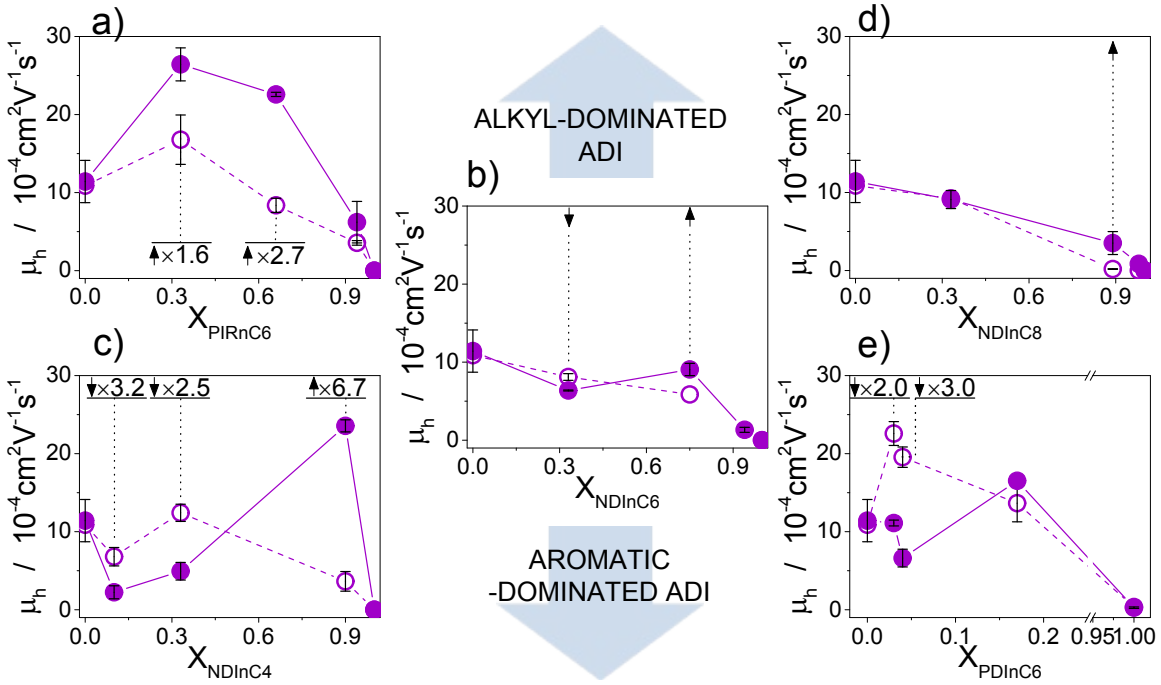

Figure S2. OFET hole mobilities (μ_h) determined for blends of P3HT with PIRnC6 (a), NDInC6 (b), or NDInC4 (c), NDInC8 (d), and PDInC6 (e) before (hollow symbols) and after (full symbols) solvent vapor annealing. X_{ADI} denote weight fractions of the respective ADIs in the blends. Lines between the symbols serve as guides to the eye. The numbers preceded with multiplication signs (×) indicate the magnitude of change in the μ_h after the solvent vapor annealing. Down arrows (↓) indicate drops whereas up arrows (↑) denote increases in μ_h after the solvent vapor annealing. Arrows without numbers indicate insignificant but noticeable tendencies of μ_h observed after the solvent vapor annealing.

Table S3. Hole and electron mobilities of all the blends and pristine materials in the study. "–" mark denotes "not observed"

Components	P3HT:ADI ratio	hole mobility [10^{-4} cm^2/Vs]		electron mobility [10^{-4} cm^2/Vs]	
		as cast	solvent annealed	as cast	solvent annealed
P3HT	1:0	10.9	11.4	–	–
P3HT:PIRnC6	**2:1**	**16.8**	**26.4**	–	–
P3HT:PIRnC6	**1:2**	**8.4**	**22.6**	–	–
P3HT:PIRnC6	**1:16**	**3.6**	**6.2**	–	–
PIRnC6	**0:1**	–	–	**0.08**	**0.52**
P3HT:NDInC4	9:1	6.8	2.2	–	–
P3HT:NDInC4	2:1	12.4	4.9	–	–
P3HT:NDInC4	1:9	3.6	23.6	–	–
NDInC4	0:1	–	–	2.3	12.3
P3HT:NDInC6	**2:1**	**8.1**	**6.4**	–	–
P3HT:NDInC6	**1:3**	**5.9**	**9.1**	–	–
P3HT:NDInC6	**1:16**	–	**1.3**	–	–
NDInC6	**0:1**	–	–	**0.03**	**1.1**
P3HT:NDInC8	2:1	9.3	9.1	–	–
P3HT:NDInC8	1:8	0.2	3.5	–	–
P3HT:NDInC8	1:40	–	0.9	4.9	–
NDInC8	0:1	–	–	53	0.25
P3HT:PDInC6	**37:1**	**22.6**	**11.1**	–	–
P3HT:PDInC6	**25:1**	**19.6**	**6.6**	–	–
P3HT:PDInC6	**5:1**	**13.7**	**16.5**	–	–
PDInC6	**0:1**	–	–	**0.35**	**0.74**

6. Exemplary deconvolution of X-ray diffraction profile and calculation of Scherrer domain sizes

The Scherrer domain sizes (t_{hkl}) were determined from full-widths at half maxima (Δq_{hkl}) of most prominent diffraction peaks of blends components, i.e. 100 peaks of P3HT and 001 peaks of ADI. The t_{hkl} were calculated from the general Scherrer formula:

$$t_{hkl} = \frac{2\pi K}{\Delta q_{hkl}}$$

Assuming the typical Scherrer constant (K) equal to 0.9. The exemplary data processing – integration and deconvolution is shown in Figure S3.

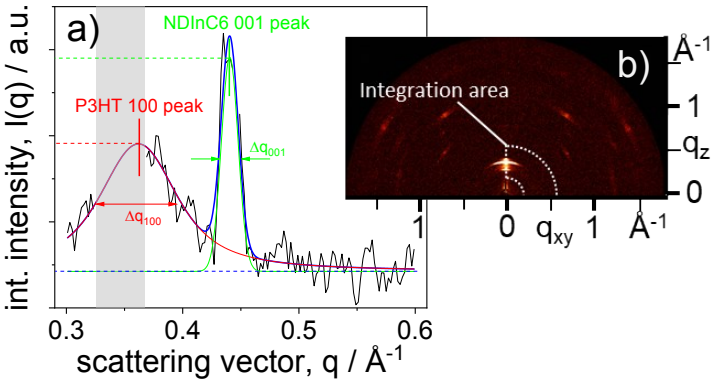

Figure S3. Exemplary deconvolution of one-dimensional I(q) profile (a) integrated from 2D-GIXD pattern (b) of P3HT:NDInC6 2:1 blend (the integration area is marked in the pattern)**.** Black, red, green and blue lines in the a panel denote, respectively: integrated experimental curve, P3HT 100 peak fit, NDInC6 001 peak fit, and cumulative fitted curve. The peaks were fitted with Voigt functions. The grey area in the I(q) profile marks the data range containing strong interference peak excluded from the analysis. The peak positions was assumed according to the reported unit cell parameters of bulk ADI crystals and the parameters unit cell of P3HT reported for thin films.[10]

7. Evolution of UV-VIS spectra of P3HT solution (1 mg/mL) over storing time

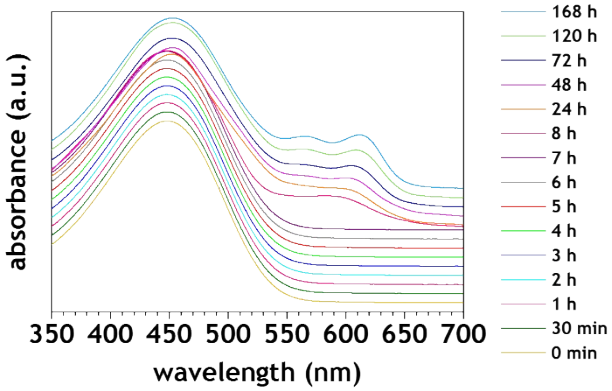

Figure S4. Series of UV-VIS spectra recorded for 1 mg/mL solution of P3HT stored at 25°C in chloroform. For clarity, the spectra are vertically shifted.

8. Exemplary deconvolution of one-dimensional X-ray diffraction pattern and the method to calculate relative degree of crystallinity

The crystallinity index of P3HT (X_c^{XRD}) were calculated from the formula:

$$X_c^{XRD} = \frac{A_c}{A_c + A_a}$$

where A_c is the total area of crystalline diffraction peaks originating from P3HT and A_a is the area of P3HT amorphous halo. The exemplary data deconvolution is shown in Figure S5.

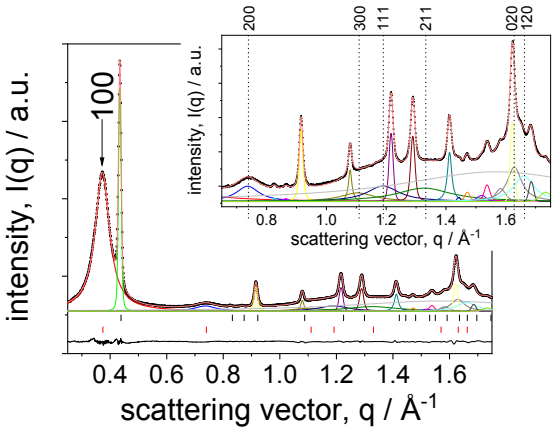

Figure S5. Exemplary deconvolution of one-dimensional I(q) profile (black points) of P3HT:NDInC6 2:1 blend. Red and black lines in the a panel denote, respectively: cumulative fitted curve and difference curve. The peaks were fitted with Voigt functions. Positions diffraction peaks of bulk P3HT and ADI were adapted from literature.[5, 11] Vertical dotted lines in the inset mark positions of P3HT peaks; the numbers denote Miller indices of the peaks.

9. Crystallography of PIRnC6 and NDInC8

A plank-shape single crystals of PIRnC6 and NDInC8 suitable for single-crystal X-ray diffraction were grown by slow evaporation of a solution in chloroform. The diffraction data were collected at 293 K with an Oxford Diffraction SuperNova diffractometer using Cu Kα radiation (λ = 1.54184 Å). Additionally, for crystals of NDInC8 the measurement was carried at 130 K. During recrystallization of PIRnC6 also the second kind of crystal, a needle-shape, was obtained and identified as the *β*-form of PIRnC6. The diffraction measurement for those crystals was performed at 130 K. The intensity data were collected and processed using CrysAlis PRO software.[12] The structures were solved by direct methods with the program SHELXT 2018/2 and refined by full-matrix least-squares method on F2 with SHELXL 2018/3.[13] The carbon-bound hydrogen atoms were refined as riding on their carriers and their displacement parameters were set equal to 1.5Ueq(C) for the methyl groups and 1.2Ueq(C) for the remaining H atoms. A summary of the crystallographic data is given in Table S4. Molecular graphics were generated with Olex2[14] and Mercury CSD 4.3.1 software.[15] ORTEP representation of the molecular structures of the reported compounds are presented in Figure S6-S8.

The measurement for PIRnC6 was carried at 293 K at which temperature the aliphatic chains of molecule were found disordered as showed in Figure S6b) (refined site occupancy factors for both positions are 0.51 and 0.48). For alkyl groups the C-C distances was fixed with DFIX 1.54 0.01 restrain. Additionally, for disordered part the DELU and ISOR restrains was used. The molecule is not centrosymmetric and geometry of aliphatic chains is differ. In crystal structure the aromatic systems and aliphatic chains are separated from each other Figures S6c) and S5d).

In the crystals of *β*-PIRnC6 asymmetric unit cell consist of two halves of molecules in special positions. In contrast to the PIRnC6, in *β*-form all the alkyl chains are extended in the trans conformation. In crystal structure molecules A and B form the alternating layers (Figure S7b) and S7c). It is worth emphasizing that there is observed the interaction between the aromatic system and the aliphatic chain of molecules from adjacent layers (Figure S7d).

The structure of the compound NDInC8 was solved on the basis of a powder experiment by Milita *et al.*[16] and the authors noted the elongation of the c parameter as a result of increase of measurement temperature. We determined the crystal structure of NDInC8 based on monocrystal measurement. Crystal was twinned and refined BASF value was 0.28. In refinement DELU and RIGU restrains was used. As observed in crystal structure of PIRnC6, the aromatic systems and aliphatic chains are in crystal separated from each other (Figure S8c). Additionally we decided to compare the unit cell parameter determined at room and low (130 K) temperature. As expected, when the temperature decreased, the length of the unit cell parameters changed and the largest change concerned the c parameter (22.71 Å at 293 K and 21.58 Å at 130 K). We did observe neither the polymorphic transformation nor changes in the arrangement of molecules in the crystal depending on temperature are presented in Figure S8d).

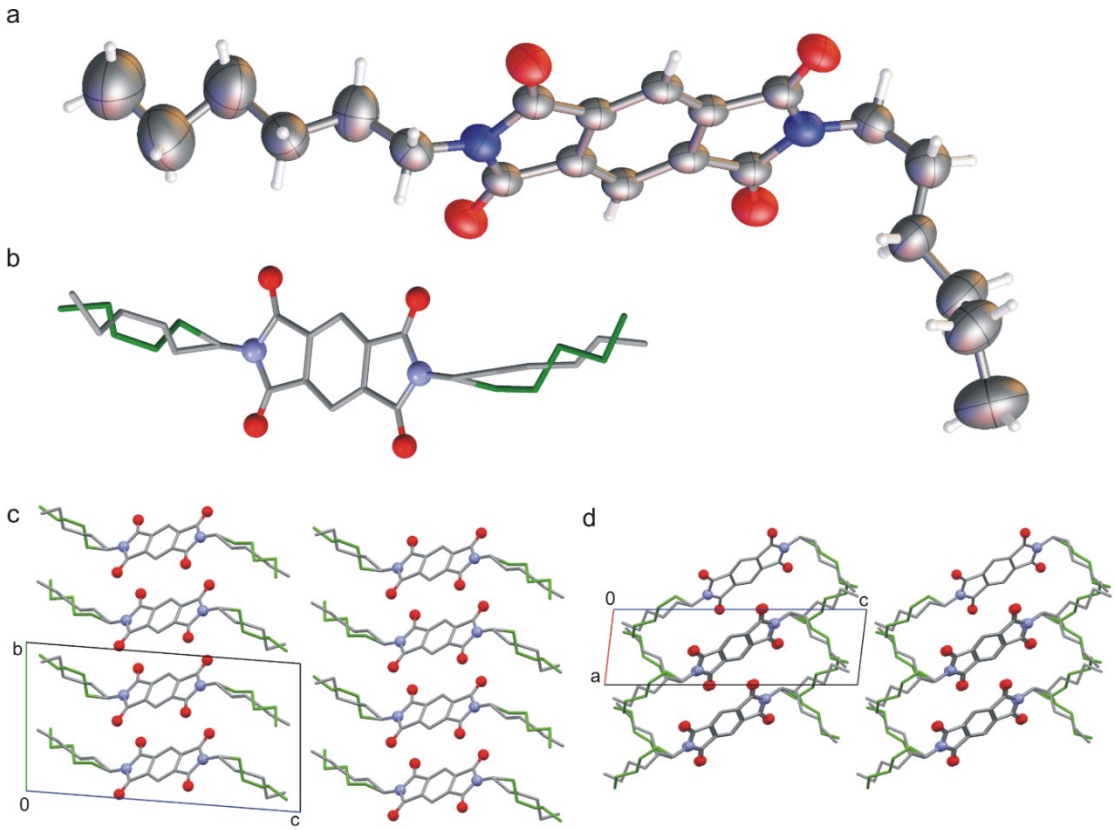

Figure S6. a) Molecular structure of PIRnC6 in crystal; only one position of disordered atoms is presented, b) the C-chain disorder mode (the green lines shows the alternative arrangement of the chains). Molecular packing in crystal structure c) view along a-axis and d) view along b-axis. The O and N atoms are showed as a balls and hydrogen atoms are omitted for clarity.

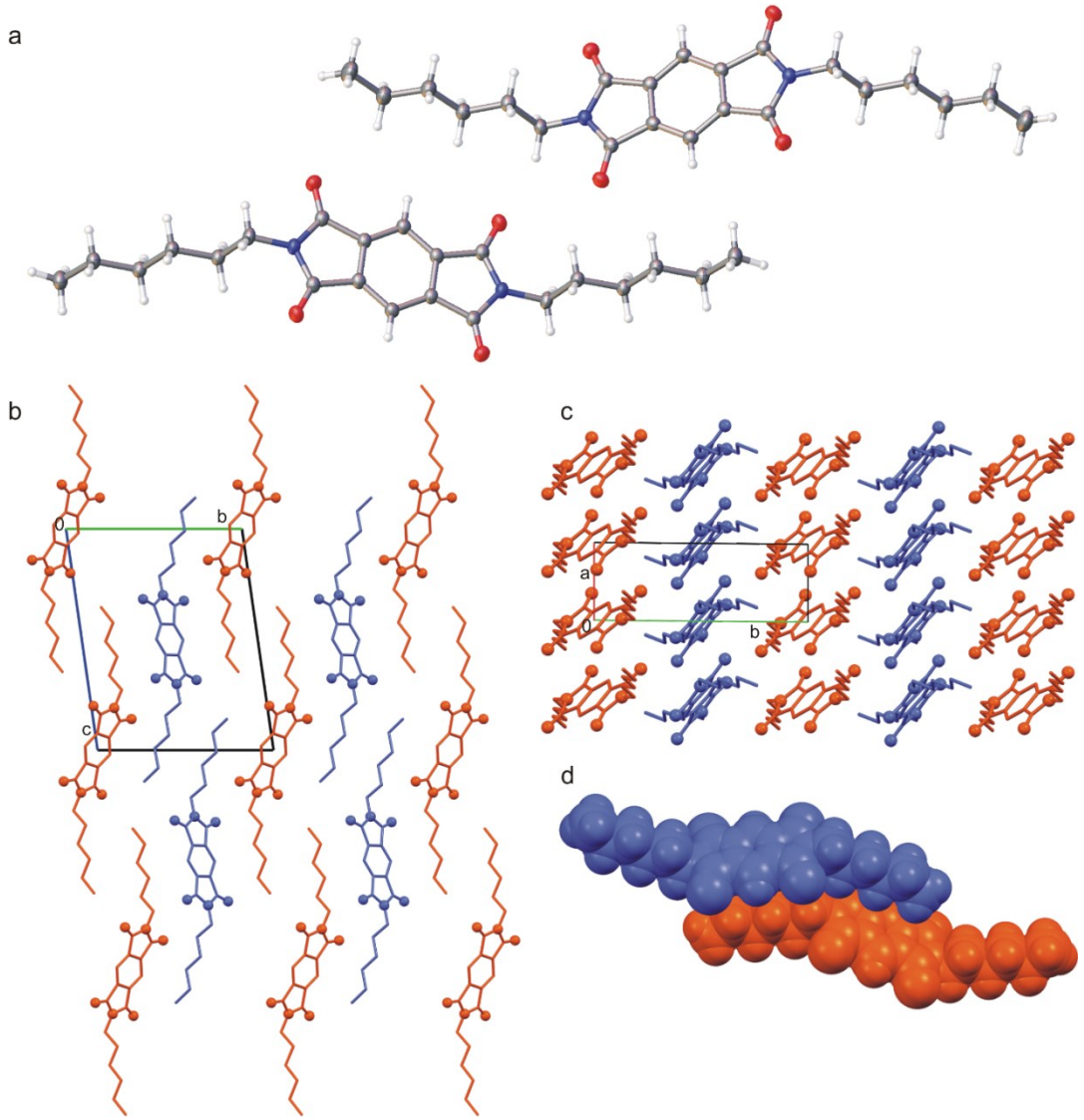

Figure S7. a) Molecular structure of asymmetric unit of *β*-PIRnC6 in crystal. Molecular packing in crystal structure c) view along a-axis and d) view along c-axis. The O and N atoms are showed as a balls and all hydrogen atoms are omitted for clarity. d) Intermolecular interactions of symmetrical independent molecules in crystal structure.

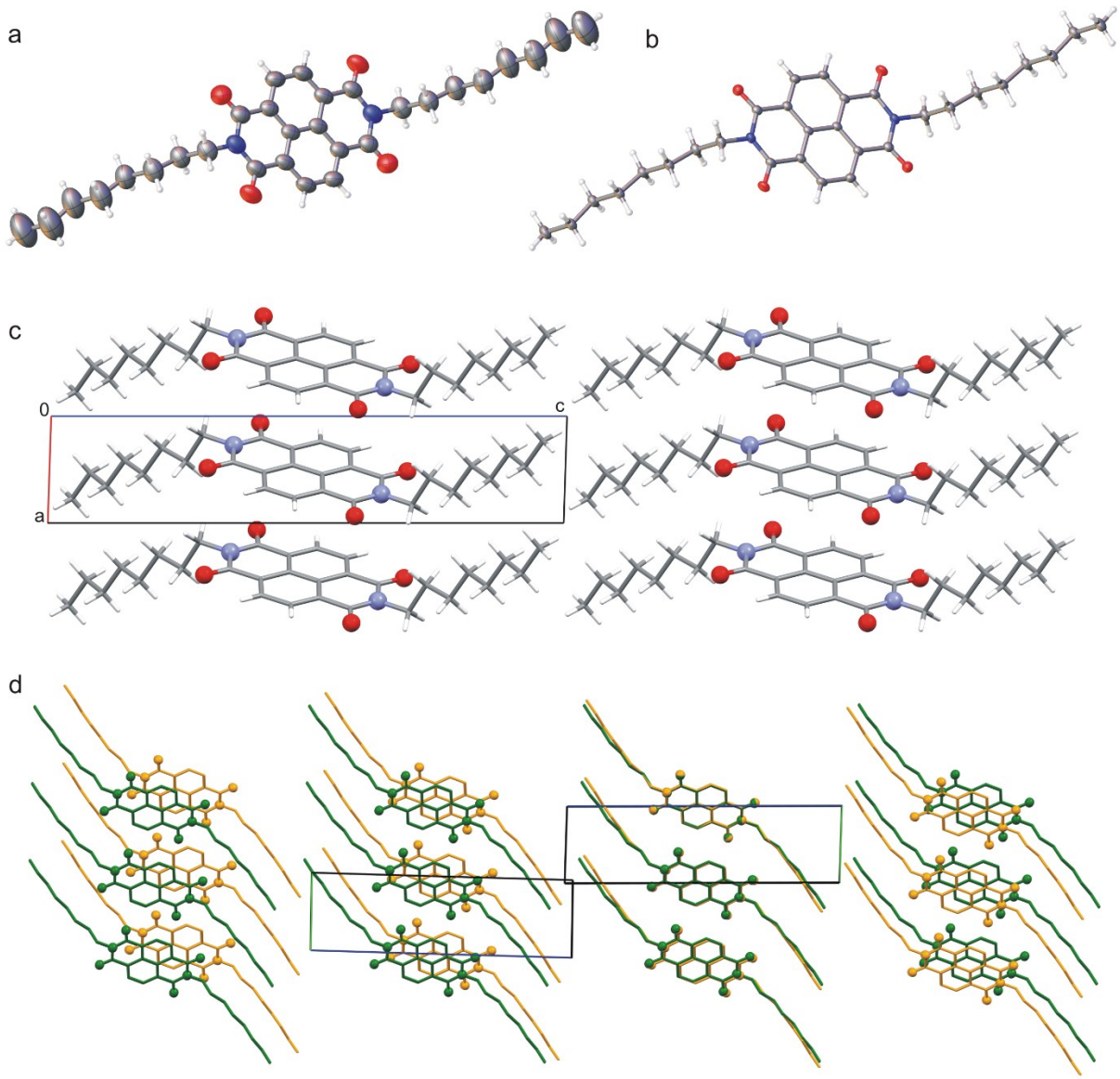

Figure S8. Molecular structure of NDInC8 in crystal structure a) at 293 K and b) at 130 K. c) Molecular arrangement in crystal structure view along b-axis. d) Comparison of molecular packing in crystal at 293 K (green) and at 130K (yellow); all hydrogen atoms are omitted for clarity. The O and N atoms are shown as balls.

Table S4. Selected crystal data and structure refinement details for PIRnC6 and NDInC8.

	PIRnC6	*β*-PIRnC6	**NDInC8**	NDInC8
CCDC number	*1998574*	*1998577*	*1998575*	*1998576*
Chemical formula	$C_{22}H_{28}N_2O_4$	$C_{22}H_{28}N_2O_4$	$C_{30}H_{38}N_2O_4$	$C_{30}H_{38}N_2O_4$
Mr	384.46	384.46	490.62	490.62
Crystal system,	Triclinic	Triclinic	Triclinic	Triclinic
space group	$P\bar{1}$	$P\bar{1}$	$P\bar{1}$	$P\bar{1}$
Temperature (K)	293 K	130 K	293 K	130 K
a, *b*, *c* (Å)	5.6790 (2),	4.6995 (2),	4.7732 (1),	4.6210 (2),
	10.1659 (6),	13.0120 (4),	6.5321 (2),	6.6424 (2),
	18.9266 (11)	16.5659 (4)	22.7126 (6)	21.5809 (10)
α, β, γ (°)	94.391 (5),	81.879 (2),	87.963 (2),	90.464 (3),
	96.784 (4),	86.016 (2),	88.858 (2),	91.624 (4),
	90.231 (4)	89.894 (3)	75.759 (2)	104.599 (3)
V (Å^3)	1081.74 (10)	1000.39 (6)	685.92 (3)	640.69 (5)
Z	2	2	1	1
D_x (Mg m^{-3})	1.180	1.276	1.188	1.272
Radiation type	Cu *K*α	Cu *K*α	Cu *K*α	Cu *K*α
μ (mm^{-1})	0.66	0.71	0.63	0.67
Crystal size (mm)	0.40 × 0.15 × 0.02	0.40 × 0.02 × 0.01	0.30 × 0.15 × 0.02	0.50 × 0.20 × 0.05
No. of measured,	7473,	15546,	4721,	8306,
independent and	4044,	4109,	4721,	2433,
observed [$I > 2\sigma(I)$]	2998	3473	3558	2115
reflections				
R_{int}	0.028	0.028		0.027
$R[F^2 > 2\sigma(F^2)]$,	0.070, 0.244, 1.09	0.039, 0.111, 1.06	0.055, 0.187, 1.06	0.045, 0.147, 1.04
$wR(F^2)$, *S*				
No. of parameters	344	255	165	164
$\Delta\rangle_{max}$, $\Delta\rangle_{min}$ (e Å^{-3})	0.18, -0.16	0.21, -0.21	0.17, -0.15	0.27, -0.27

10. Supporting references

1. C. Li, K. Han, J. Li, H. Zhang, J. Ma, X. Shu, Z. Chen, L. Weng and X. Jia, *Org. Lett.*, 2012, **14**, 42-45.
2. P. M. Alvey, J. J. Reczek, V. Lynch and B. L. Iverson, *J. Org. Chem.*, 2010, **75**, 7682-7690.
3. Y. Matsunaga, K. Goto, K. Kubono, K. Sako and T. Shinmyozu, *Chem. Eur. J.*, 2014, **20**, 7309-7316.
4. J. J. Reczek, K. R. Villazor, V. Lynch, T. M. Swager and B. L. Iverson, *J. Am. Chem. Soc.*, 2006, **128**, 7995-8002.
5. Y. Ofir, A. Zelichenok and S. Yitzchaik, *J. Mater. Chem.*, 2006, **16**, 2142-2149.
6. B. Baumgartner, A. Svirkova, J. Bintinger, C. Hametner, M. Marchetti-Deschmann and M. M. Unterlass, *Chem. Commun.*, 2017, **53**, 1229-1232.
7. J. Pitchaimani, A. Kundu, S. P. Anthony, D. Moon and V. Madhu, *ChemistrySelect*, 2020, **5**, 2070-2074.
8. D. Shukla, S. F. Nelson, D. C. Freeman, M. Rajeswaran, W. G. Ahearn, D. M. Meyer and J. T. Carey, *Chem. Mater.*, 2008, **20**, 7486-7491.
9. E. Iengo, G. D. Pantoş, J. K. M. Sanders, M. Orlandi, C. Chiorboli, S. Fracasso and F. Scandola, *Chem. Sci.*, 2011, **2**, 676-685.
10. M. El Gemayel, A. Narita, L. F. Dossel, R. S. Sundaram, A. Kiersnowski, W. Pisula, M. R. Hansen, A. C. Ferrari, E. Orgiu, X. Feng, K. Müllen and P. Samori, *Nanoscale*, 2014, **6**, 6301-6314.
11. D. Dudenko, A. Kiersnowski, J. Shu, W. Pisula, D. Sebastiani, H. W. Spiess and M. R. Hansen, *Angew. Chem. Int. Ed.*, 2012, **51**, 11068-11072.
12. CrysAlis PRO *In Rigaku Oxford Diffraction 1.171.40.57a, ed.; 2019*
13. G. Sheldrick, *Acta Crystallographica Section A*, 2015, **71**, 3-8.
14. O. V. Dolomanov, L. J. Bourhis, R. J. Gildea, J. A. K. Howard and H. Puschmann, *J. Appl. Crystallogr.*, 2009, **42**, 339-341.
15. C. F. Macrae, I. Sovago, S. J. Cottrell, P. T. A. Galek, P. McCabe, E. Pidcock, M. Platings, G. P. Shields, J. S. Stevens, M. Towler and P. A. Wood, *J. Appl. Crystallogr.*, 2020, **53**, 226-235.
16. S. Milita, F. Liscio, L. Cowen, M. Cavallini, B. A. Drain, T. Degousée, S. Luong, O. Fenwick, A. Guagliardi, B. C. Schroeder and N. Masciocchi, *J. Mater. Chem. C*, 2020, **8**, 3097-3112.